Combined Admittance Control with Type II Singularity Evasion for Parallel Robots using Dynamic Movement Primitives

Rafael J. Escarabajal, José L. Pulloquinga, Ángel Valera, *Member, IEEE*, Vicente Mata, Marina Vallés and Fernando J. Castillo-García

***Abstract*—This paper addresses a new way of generating compliant trajectories for control using movement primitives to allow physical human-robot interaction where parallel robots (PRs) are involved. PRs are suitable for tasks requiring precision and performance because of their robust behavior. However, two fundamental issues must be resolved to ensure safe operation: i) the force exerted on the human must be controlled and limited, and ii) Type II singularities should be avoided to keep complete control of the robot. We offer a unified solution under the Dynamic Movement Primitives (DMP) framework to tackle both tasks simultaneously. DMPs are used to get an abstract representation for movement generation and are involved in broad areas such as imitation learning and movement recognition. For force control, we design an admittance controller intrinsically defined within the DMP structure, and subsequently, the Type II singularity evasion layer is added to the system. Both the admittance controller and the evader exploit the dynamic behavior of the DMP and its properties related to invariance and temporal coupling, and the whole system is deployed in a real PR meant for knee rehabilitation. The results show the capability of the system to perform safe rehabilitation exercises.**

***Index Terms*—Dynamic movement primitives, Force control, Parallel robot, Rehabilitation robotics, Singularity avoidance**

I. Introduction

HUMAN-ROBOT interaction is a multidisciplinary field that includes industrial, social, and medical applications [1]. In the latter category, rehabilitation is one of the leading applications [2], which entails physical interaction to assist the patient. This kind of task requires high performance and robustness to ensure safe behavior. Parallel robots (PRs) are suitable for them thanks to their stiffness, load capacity, and accuracy [3], and usually consist of a fixed platform and a controlled mobile platform which are linked by closed kinematic chains [4]. Specifically, lower limb rehabilitation with PRs has been deeply studied recently [5]–[7], and it is the central application of this paper.

Physical interaction in rehabilitation tasks must be safe and no pain has to be induced to the patient. In this regard, admittance control is one of the main strategies [8], which generates robot motion based on the human force, so the end-effector tracks an admittance model. Some applications of admittance control in lower limb rehabilitation can also be found in [9], [10]. However, this generated motion from the human input raises a new problem in PRs: the admittance controller may lead the robot to a Type II singular configuration inside its workspace due to the fact that the force control may need to change the a priori trajectory to keep compliant interaction, so even if the original designed trajectory was free of singularities, the resulting one can reach singular configurations unpredictably. In this case, the control of the mobile platform is lost, and the patient's safety could be in risk.

Gosselin and Angeles [11] established a classification of singular configurations in PRs, which divides them into two categories: on the one hand, in Type I or inverse kinematic singularities, at least one degree of freedom (DOF) is lost because the determinant of the inverse Jacobian matrix becomes null. This kind of singularity typically occurs in serial robots and usually corresponds to the end-effector of the robot operating at the boundaries of the workspace. On the other hand, Type II singularities imply the gain of at least one uncontrolled DOF because of the degeneracy of the forward Jacobian matrix, meaning that the PR cannot bear external forces despite the actuators being locked, and they may occur inside the workspace, making them harder to address [12].

The negative effect of this kind of singularity is emphasized when combined with an admittance control since i) the human participates in the motion of the mobile platform, so there is a factor of uncertainty in the resulting position, with the possibility of getting into a singular configuration, and ii) if the PR effectively reaches a singular configuration, its response becomes unpredictable in the presence of a force that the human may presumably be exchanging since such force is unbearable for the PR. For those reasons, it is imperative to address the treatment of Type II singularities when designing a force controller for a PR.

Some methods to tackle this problem can be found in literature, starting from the mechanical design process of the PR by optimizing its workspace [13], [14]. However, this is not

This research was partially funded by Fondo Europeo de Desarrollo Regional (PID2021-125694OB-I00), cofounded by Vicerrectorado de Investigación de la Universitat Politècnica de València (PAID-11-21) and by Ministerio de Universidades, Gobierno de España (FPU18/05105).

Rafael J. Escarabajal, José L. Pulloquinga, Ángel Valera and Marina Vallés are with the Departamento de Ingeniería de Sistemas y Automática, Instituto de Automática e Informática Industrial, Valencia, Camino de Vera, s/n, Spain (e-mail: raessan2@doctor.upv.es; jopulza@doctor.upv.es; giuprog@isa.upv.es; mvalles@isa.upv.es)

Vicente Mata is with the Universitat Politècnica de València, Departamento de Ingeniería Mecánica y de Materiales, Centro de Investigación en Ingeniería Mecánica, Valencia, Camino de Vera, s/n, Spain (e-mail: vmata@mcm.upv.es)

Fernando J. Castillo-García is with the Universidad de Castilla-La Mancha, Escuela de Ingeniería Industrial, Av. Carlos III s/n, 45071, Ciudad Real, Spain (e-mail: fernando.castillo@uclm.es)

enough to ensure a complete singular-free workspace and so the singularity analysis is still a concern. The characterization of Type II singularities has also been researched, and methods based on Screw Theory [15] have been proposed [16]–[18] since the Jacobian alone does not provide enough physical information. Some works have been developed using these kinds of techniques to help a PR deal with singularities during operation, requiring extra sensorization such as vision systems since the robot's kinematic model is no longer valid in the vicinity of a singularity [19].

Both the admittance controller and the singularity evader rely on the idea of altering the reference position signal to fulfill their goal. Dynamic Movement Primitives (DMP) [20], [21] is a mechanism that provides a representation of motions in parallelism with biological systems by encoding the reference signal using nonlinear dynamical systems, aiming at the generation of trajectories for control and planning. DMPs are composed of a set of differential equations with attractor properties and a nonlinear learnable component with several advantages [22], like providing a framework for imitation learning [23], movement generation and recognition [24], generalization to different targets [25], modulation of the system with techniques like slow-down feedback [26], and a reactive behavior using coupling actions [21]. They have been implemented for tasks like cooperative interaction with the environment [27] or obstacle avoidance [28].

In this paper, the desired behavior in terms of admittance and singularity evasion is embedded into a DMP system through the aforementioned coupling actions. The admittance behavior can be seen as an instance of interaction with the environment, while the Type II singularity avoidance can be treated to some extent as obstacle avoidance. However, this paper proposes a novel approach for the avoidance that involves the detection of the two limbs which most contribute to the singular configuration and adapting the reference trajectory of these limbs with the help of the DMP by defining the coupling actions from the output of an additional embedded controller to fulfill a tracking objective, rather than blindly applying repulsive actions that could degrade the performance.

In most works, the parameters of the DMP (corresponding to the equivalent damping and stiffness of a second-order dynamical system) are given some fixed or standard values to ensure critically damped or overdamped behavior [21]. However, they do not dig into the effect of those constants on the response regarding the coupling action received. In this research, a new insight into the DMP is provided where we design those parameters to obtain the intended behavior when feeding the coupling action. The unified system proposed in this paper can exploit all the advantages of DMPs while ensuring the compliant response of the robotic system.

The whole purpose and the contribution of this paper is the tracking of position and force reference profiles while avoiding Type II singularities with a PR, both tasks exploiting the DMP advantages and dynamic behavior. There exist methods for offline planning trajectories free of singularities [29], which cannot adapt to online changes like those happening with force control. Also, some strategies have been proposed to cross singular configurations [30]. However, crossing a singularity in a human-robot interaction setting may not be the safest solution because of the combined effect of a control loss and external force exertion. In [19] the task of singularity releasing was performed, meaning that the PR was initially inside a singular configuration and the controller had to drive the PR out of the singularity safely, as opposed to evasion, in which the PR has to continuously replan trajectories free of singularities to avoid getting into them. To the best of the authors' knowledge, very little has been developed regarding Type II singularity evasion online, and exclusively for redundant robots [31], [32]. However, these robots are not exempted from singular configurations and a careful study of the workspace is required, arising new problems related to the complex modelling they involve.

The method presented in this paper is useful in environments of safe-critical operation such as rehabilitation with non-redundant parallel robots, where trajectories cannot be totally planned beforehand since the interaction between human and robot must remain compliant. The role of the DMP is to provide the required online adaptation of the reference trajectory with respect to the reference baseline in order to achieve both compliant behavior and singularity avoidance. DMPs exhibit advantageous properties for this purpose, like incremental learning (possibility to adapt to changes of the trajectory), and reactive behavior using coupling actions. This paper also explores a new way to design the coupling actions based on a novel mechanism that uses a DMP-embedded controller, which provides minimum deviation from the original defined trajectory and has not been found for similar tasks.

After the related work in Section II, the formulation of our version of the DMP and its dynamical properties are explained in Section III. Section IV depicts the admittance controller by including its coupling term, and Section V presents the Type II singularity avoidance layer, which is treated as a new coupling action. In Section VI, the combined system for control is designed. Section VII describes the setup for the experiments, including the 4-DOF PR for knee rehabilitation and the sensors and software requirements. The test trajectories and the results of the robot performance for those trajectories are also depicted. Finally, the conclusions are presented in Section VIII.

II. Related work

Lower-limb rehabilitation robotics is an emerging field from which several novel mechanisms have been developed recently [7], [33], [34], many of them involving the use of PRs. First attempts to use the force feedback for changing the robot's position were reported by Hogan [35]. However, the combination of force feedback with DMPs has been barely explored. Gams et al. [27] designed cooperative DMPs using coupling terms learned using iterative learning control [36]. Shahriari et al. [37] developed a framework consisting of a DMP for trajectory encoding and an admittance controller to track wrench profiles with a virtual energy tank to guarantee passivity, and Kramberger et al. [38] added to that framework a direct coupling of the admittance dynamics into the DMP. This work is the most similar approach to ours; however,

they still rely on the design of the coupling term rather than the DMP structure. Wang et al. [39] presented a framework for robot learning with a teaching phase, learning phase, and reproduction phase, in which an adaptive admittance controller was used to account for the unknown human dynamics, and a neural network-based controller was developed to track the trajectories from the motion model. DMPs and Gaussian mixture regression were used to encode the human characteristics based on their demonstrations [40].

On the other hand, Type II singularity detection and avoidance has traditionally been treated as an isolated topic, not related to admittance control or DMPs. Agarwal et al. [41] designed a control scheme to modify the behavior of a planar PR in the proximity of a singularity employing artificial potential functions at the cost of one DOF of the PR. Six et al. [30] proposed a new method to cross singularities by modifying the dynamic model and a computed-torque control law. These studies have in common that joint positions are sensed to estimate the cartesian position. Nevertheless, that is not the safest solution since the direct kinematic model becomes inaccurate in the vicinity of a singularity. Recently, Pulloquinga et al. [19] measured the cartesian position of a 4-DOF PR directly by means of a vision system and used that information to release a PR from an initial singular configuration. The algorithm used information not only from the Jacobian but also from the Output Twist Screws (OTSs) [18] as a proximity detector. The algorithm geometrically chooses the two actuators that mostly participate in the singularity and change their reference linearly until the PR gets released from the singular configuration. In this study, that method is extended so that the evasion action, instead of affecting the reference signal directly in a linear fashion, uses controlled actions embedded in a coupling term of the DMP to achieve smoother transitions, resembling the obstacle avoidance methods that have been implemented with DMPs [42].

III. Dynamic Movement Primitives as a Mass-Spring-Damper System

A. Formulation

The DMP structure has been expressed in literature as a spring-damper second-order dynamical system, stimulated with a nonlinear forcing term [43], [44]. In this study, that formulation is extended to a mass-spring-damper dynamical system so that the full dynamical behavior can be controlled, and it is expressed for one DOF as follows:

$$\begin{aligned} \tau M\dot{z} &= K(g-y) - Dz + f(x) \\ \tau\dot{y} &= z \end{aligned} \tag{1}$$

where y is the position and z the scaled velocity by the temporal factor τ that allows speed changes, which is initially equal to the temporal length of the trajectory, and g is the goal (final) position and the attractor point, with $z = 0$. Regarding the dynamical system, M is the mass constant, K is the spring constant, and D is the damping term. The nonlinear function f is dependent on a phase variable x instead of time directly, and is defined as a linear combination of N radial basis functions as follows:

$$f(x) = \frac{\sum_{i=1}^{N} w_i \Psi_i(x)}{\sum_{i=1}^{N} \Psi_i(x)} x \tag{2}$$

$$\Psi_i(x) = \exp(-h_i(x - c_i)^2) \tag{3}$$

where c_i are the centers of the radial basis functions distributed along the trajectory and h_i the bandwidths. The weights w_i are learned to fit the function, and the phase replaces time and obeys the following first-order linear dynamical system:

$$\tau\dot{x} = -\alpha_x x \tag{4}$$

where α_x is a positive time constant corresponding to the exponential decay of the dynamical system. For this system, $x(0) = 1$ and x tends to 0 with the law $x(t) = \exp(-\alpha_x t/\tau)$. Unlike time, the phase variable can be conveniently modified during execution. The weights w_i are learned using techniques like Locally Weighted Regression (LWR) [45]. In the case of multiple DOFs, each has its own DMP system and forcing terms, but they are all synchronized by the same canonical system.

In traditional DMPs, the values K and D of the DMP are fixed in advance to some standard values to ensure the system's convergence and critically-damped behavior. However, this paper proposes a new method to conveniently define those parameters (and M, which has not been taken into consideration before) without neglecting those issues. This approach aims to control the effect of the additional coupling terms that can be added. These coupling terms are one of the most interesting properties of DMPs and leave the system (1) as:

$$\tau^2 M\ddot{y} = K(g-y) - D\tau\dot{y} + f(x) + f_C \tag{5}$$

This system has been expressed in the alternative second-order differential equation to facilitate the posterior study, where f_C encompasses the coupling terms already used, for example, for obstacle avoidance [28], [42].

B. Design of dynamic specifications and response

The main concern now is to achieve the desired behavior from the DMP when dealing with external coupling forces. This paper proposes three dynamic constraints to obtain the constants M, K, and D from the DMP (since τ and g have fixed values). The dynamics of the system can be typically defined by the following contrains:

1) The desired static gain (G).
2) The required settling time to reach the steady state with an error band of 2% (t_s).
3) The critically-damped behavior of the system.

Generally, only the third constraint is considered in the literature, and the parameters are arbitrarily defined to fulfill it with a certain fast dynamics. In this study, we start with the formulation of the DMP in terms of a transfer function, with f_C as input, y as output, and s the Laplace variable. Here, we neglect the term $f(x)$ since its purpose is to define the shape of

the learned reference trajectory, and it is unambiguously given by the phase. On the other hand, the term f_C defines how much the reference is deviated from the original trajectory to accomplish user-defined requirements, hence its interest, and its effect is given by:

$$DMP(s) = \frac{Y(s)}{F_C(s)} = \frac{1}{\tau^2 M s^2 + \tau D s + K} \tag{6}$$

This dynamical system faces a problem: the parameter τ, which provides extra flexibility with the possibility of modifying the speed, also alters the dynamics (specifically, it is involved in constraints 2 and 3). Moreover, this parameter depends on the duration of the trajectory, so changing the trajectory would alter the dynamic response. To alleviate this problem, we start by comparing the system with a standard mass-spring-damper system, whose transfer function is:

$$\frac{Y(s)}{F(s)} = \frac{1}{ms^2 + ds + k} \tag{7}$$

where m, d, k are the mass, damping and spring constants of the standard mass-spring-damper system, respectively. This system has well-known dynamic properties and can be used as a baseline for simultaneously satisfying constraints 1-3. In fact, there are three constraints and three variables (m, d, k), making it a determinate compatible system whose solution is (see Appendix A):

$$k = \frac{1}{G}, \qquad d = \frac{t_s k}{2}, \qquad m = \frac{d^2}{4k} \tag{8}$$

This result must be extrapolated from a standard spring-damper system to the DMP just by equating equations (6) and (7):

$$M = \frac{m}{\tau^2}, \qquad D = \frac{d}{\tau}, \qquad K = k \tag{9}$$

As demonstrated above, the parameter τ is the one that differentiates a conventional mass-spring-damper system with a DMP. The design of a DMP neglecting this issue leads to negative consequences; for example, makes the dynamics dependent on the duration of the trajectory. On the other hand, this parameter cannot be dropped since we would lose the capabilities for changing the speed, and also it regulates the canonical system (equation (4)). Therefore, the workflow to obtain the desired responses implies:

1) Choosing the desired static gain (G) and settling time (t_s) for the experiment.
2) Defining the parameters k, d, and m for a standard mass-spring-damper model to follow that behavior using equation (8).
3) Calculating M, D, and K for the DMP from equations (9).
4) Learning the trajectory in a conventional way with equations (1)-(4).
5) Running the DMP by performing the integration of the subsystems (the phase and the mass-spring-damper) taking into account the coupling actions f_C occurring along the trajectory for reference adaptation.

For many DOFs, both vectors $\vec{G}$ and $\vec{t_s}$ with lengths equal to the number of DOFs are defined, and the computations are performed element-wise, obtaining $\vec{M}$, $\vec{D}$, and $\vec{K}$, which allow different behaviors for each DOF according to the needs, but still synchronized by the same canonical system.

Finally, it is worth mentioning that the stability of the new system is ensured with bounded coupling forces and parameters satisfying constraints 1-3 with a position controller thanks to the DMP properties [46], and the system converges to the goal g.

IV. Admittance control based on coupling forces

The first and most obvious way to take advantage of the novel version of the DMP is to exploit the user-defined mass-spring-damper behavior to use it as an admittance controller. This requires both a position and a force profile to track, which are correspondent in time and typically provided in tabulated files:

$$\mathbf{Y_d} = [[y_{\lambda t}, \dot{y}_{\lambda t}, \ddot{y}_{\lambda t}]_{\lambda=1}^{\Lambda}]_{t=1}^{T} \tag{10}$$

$$\mathbf{Q_d} = [[q_{\lambda t}, \dot{q}_{\lambda t}, \ddot{q}_{\lambda t}]_{\lambda=1}^{\Lambda}]_{t=1}^{T} \tag{11}$$

$$\mathbf{F_d} = [[F_{\lambda t}]_{\lambda=1}^{\Lambda}]_{t=1}^{T} \tag{12}$$

where $\mathbf{Y_d}$ gathers the reference in cartesian space and $\mathbf{Q_d}$ in joint space, with λ the current DOF, Λ the total number of DOFs, t the time instant, and T the number of samples of the trajectory. Regarding the reference $\mathbf{Y_d}$, we assume in this work that the orientation is characterized by the Euler angles and their derivatives, so $\mathbf{Y_d}$ contains these variables rather than angular velocities. This means that we can keep the same DMP structure instead of using the quaternion-based orientation DMP described in [47]. This setup has the advantage of controlling the dynamic behavior independently in each rotation axis.

The forces are typically provided in cartesian coordinates for the end effector since it is the part of the robot interacting with the environment. From this point, the λ subscript is dropped to keep the notation uncluttered, and the scalar version is used (as we did with the DMP formulation) since the vector version applies the same procedure for every DOF.

The desired position is encoded with a DMP, which no longer ensures the time synchronization with the force sampled from the file. For that reason, forces are sampled instead from a synchronized encoded system consisting of a linear combination of N_F basis functions (i.e., a Gaussian Kernel Approximator, GKA) affected by the same phase x as the position [48]:

$$F_{ref}(x) = \frac{\sum_{i=1}^{N_F} w_i^F \Psi_i^F(x)}{\sum_{i=1}^{N_F} \Psi_i^F(x)} x \tag{13}$$

where the superscript F makes the distinction with respect to the basis functions and weights from the position encoding of equation (2). The subscript of the force F_{ref} is different

from the one of equation (12) (F_d) to emphasize that this force comes from the approximation rather than the initial file.

The coupling term is thus the difference between the force reference and the force measured by the sensor:

$$f_C = e_F = F_{ref} - F_{meas} \tag{14}$$

This coupling term provokes the desired effect on the system by defining the proper M, D, and K constants for the DMP as described in Section III-B. Any kind of controller can be employed as the underlying position controller, and in this study, we use a proportional-derivative controller with gravity compensation (PD+G).

Figure 1 represents the scheme of the admittance controller intrinsically embedded into the DMP system. The DMP is encoded using cartesian coordinates to match those of the incoming coupling force. Then, inverse kinematics is applied to the output of the reference to allow joint space control ($\vec{q}_{ref}$). A saturator can be added to prevent the admittance model from pushing the joints beyond their geometrical limits ($\vec{q}_{ref,sat}$). The vectorized form is employed, and the joint position controller block (which in our case is a PD+G controller) is oversimplified for visualization purposes since it not only receives the error $\vec{e}_q$ to calculate the control action $\vec{u}$, but also the derivative of the error to calculate the derivative term and the raw position ($\vec{q}_{meas}$) for the gravitational term.

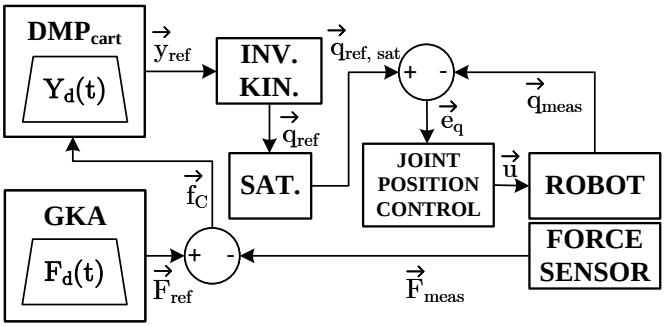

Fig. 1. DMP-embedded admittance controller defined in cartesian space with GKA for force synchronization and PD+G low-level position controller.

This controller, however, may face severe problems in PRs since the admittance model may drive a PR to a Type II singularity within the workspace. For that reason, a new coupling term is designed in Section V to allow PRs to avoid Type II singularities.

V. Type II singularities avoidance

A. Detection of Type II singularities

According to Gosselin and Angeles [11], there is a relationship between the independent generalized coordinates ($\vec{q}$) and the end effector's PR pose ($\vec{y}$) given by a set of constraint equations $\vec{\Phi}$. Taking the time derivatives of $\vec{\Phi}$, the differential kinematics can be expressed as follows:

$$J_I(\vec{q})\dot{\vec{q}} = J_D(\vec{y})\dot{\vec{y}} \tag{15}$$

where J_D is the forward or direct Jacobian matrix and J_I is the inverse Jacobian matrix, both square with size equal to the number of DOFs (Λ). In a Type I singularity, J_I becomes rank deficient ($||J_I|| = 0$) and corresponds to that of a serial robot, involving the loss of at least one DOF. On the other hand, in a Type II singularity the forward Jacobian matrix (J_D) degenerates ($||J_D|| = 0$) and the mobile platform can move in the presence of external forces even if all the actuators are locked. This analysis is justified by the fact that in human-robot interaction (for example, with an admittance controller) such external forces exist and could make the robot's behavior unpredictable and non-compliant.

As a PR approaches a Type II singular configuration, its kinematic model becomes inaccurate. For that reason, it is necessary to estimate $\vec{y}$ directly from external sensors rather than apply the forward kinematic model to the active coordinates obtained from the encoders. A vision system is a good candidate for estimating $\vec{y}$ [19].

However, $||J_D||$ alone gives no clue about the active elements responsible for the singular configuration. In [17], the mobile platform's movement ($\$$) was divided into Λ Output Twist Screws (OTSs) as follows:

$$\$ = \rho_1\hat{\$}_{O_1} + \rho_2\hat{\$}_{O_2} + \cdots + \rho_\Lambda\hat{\$}_{O_\Lambda} \tag{16}$$

where ρ_i is the amplitude of each OTS and $\hat{\$}_{O_i}$ is a normalized screw that includes the instantaneous screw axis and the linear component: $\hat{\$}_{O_i} = (\vec{\mu}_{\omega_O}; \vec{\mu}^*_{v_O})$. Each $\hat{\$}_{O_i}$ is obtained by locking the rest $\Lambda - 1$ actuators and using the normalized Transmission Wrench Screw (TWS) $\hat{\$}_T$ as follows [49]:

$$\hat{\$}_{O_i} \circ \hat{\$}_{T_j} = 0 \ (i, j = 1, 2, \ldots, \Lambda, i \neq j) \tag{17}$$

where $\circ$ is the reciprocal product. Wang and Liu [49] showed that in a Type II singularity, at least two OTSs are linearly dependent, meaning that both $\vec{\mu}_{\omega_O}$ and $\vec{\mu}^*_{v_O}$ of two $\hat{\$}_O$ are parallel. For that reason, the angle between two $\vec{\mu}_{\omega_O}$ ($\Omega_{i,j}$) is an excelent candidate for evaluating the proximity to a Type II singularity, and it can be verified with the equality of $\vec{\mu}^*_{v_O}$. For Λ $\hat{\$}_O$, there are $\binom{\Lambda}{2}$ angles Ω, defined as:

$$\Omega_{i,j} = \arccos\left(\vec{\mu}_{\omega_{O_i}} \cdot \vec{\mu}_{\omega_{O_j}}\right) \ (i, j = 1, 2, \ldots, \Lambda, i \neq j) \tag{18}$$

Unlike $||J_D||$, $\Omega_{i,j}$ is a dimensional measure, so the proximity to a Type II singularity can be measured in angular units. As $\Omega_{i,j}$ reaches 0, the PR approaches a singular configuration where i and j are the pair of chains responsible for that singular configuration [18]. An accurate calculation of $\Omega_{i,j}$ also requires a reasonable estimation of $\vec{y}$, which reinforces the idea that external sensors are needed to measure the PR's pose.

In [19], these angles were applied together with J_D to release a PR from an initial singular configuration by detecting the two limbs most responsible for that singularity (corresponding to the minimum of all the angles) and moving them in the proper direction that sooner gets the PR out of the singularity.

In this paper, we employ those indices to avoid singular configurations, i.e., prevent a PR from getting into positions with low $\Omega_{i,j}$ or $||J_D||$, in combination with the DMP and the

admittance model to allow both compliant and robust behavior simultaneously in PRs.

To perform this task, we first detect the two limbs i and j which most contribute to the singularity (corresponding to Ω_{min}) and then we design the coupling actions required to move those limbs, while keeping the rest unaltered by the coupling actions during the evasion task.

B. Design of the coupling term for singularities avoidance

Hereafter, only the minimum of the angles, Ω_{min}, is considered because of its connection to a potential singular configuration, and the PR position becomes more singular as either Ω_{min} or $||J_D||$ approach 0. For that reason, a limit for both of them, Ω_{lim} and $||J_D||_{lim}$, are defined experimentally. The coupling force acts as soon as any measurement of Ω_{min} or $||J_D||$ falls below its corresponding threshold. Only the two limbs related to Ω_{min} (named l_i and l_j, which are stacked in a vector $\vec{l}_{2\times1}$) are modified by the coupling term. Since the algorithm for singularity avoidance relies on independent movements of two joints, a DMP defined in joint coordinates is more convenient because a coupling force will directly move the desired limbs (unlike what happened in the admittance case).

The coupling action should act as a repulsive force that drives the robot to a position that is not singular (i. e., beyond the thresholds Ω_{min} and $||J_D||$), so this objective can be posed as a control problem with input f_C and goals Ω_{lim} and $||J_D||_{lim}$. These goals can be treated separately, and a PID-like control law has been chosen for each one of them, with some nuances explained in the following.

We distinguish three different situations regarding the participation of each limb η in a singular configuration:

1) If the robot is in a singular configuration and limb η is involved according to the index Ω_{min} (η is a member of vector $\vec{l}$), then the repulsion force for this limb is based on a PID controller like explained below.
2) If the robot is in a singular configuration and limb η is *not* involved according to the index Ω_{min} (η is *not* a member of vector $\vec{l}$), then its coupling force remains unchanged with respect to the previous value. This implies that if it participated in the singularity before and there was a change of responsible limbs, the force of this limb will keep acting to avoid chattering or abrupt changes. If it did not participate, its value was always 0.
3) If the robot is not in a singular configuration, the integrator of each PID will gradually decrease until zeroing the repulsion force.

The control of the angle Ω_{min} is activated when $\Omega_{min} < \Omega_{lim}$, and the following magnitude is first computed:

$$e_\Omega = 1 - \frac{\Omega_{min}}{\Omega_{lim}} \tag{19}$$

where e_Ω is a normalized tracking error for which it is convenient to scale the reference to 1 for both indicators (Ω_{lim} and $||J_D||_{lim}$). Then, for each limb involved in the singularity (elements l_i of vector $\vec{l}$), the following scalar is computed:

$$||f_C||_{\Omega_{l_i}} = K_p e_\Omega + K_d \dot{e}_\Omega + K_i[\int e_\Omega dt]_{l_i} \tag{20}$$

In this expression, K_p, K_d, and K_i are the proportional, derivative, and integral constants, respectively. However, each limb uses its own integrator, which is indicated by the nomenclature $[\int \cdots]_{l_i}$. This is useful in case of changing the responsible limbs within the same singular region, since only the responsible limbs will keep integrating, while the rest are kept unchanged. Analogously, for the determinant of the Jacobian, when $||J_D|| < ||J_D||_{lim}$ we employ:

$$e_J = 1 - \frac{||J_D||}{||J_D||_{lim}} \tag{21}$$

$$||f_C||_{J_{l_i}} = K_p e_J + K_d \dot{e}_J + K_i[\int e_J dt]_{l_i} \tag{22}$$

By the same logic, each limb has its own integrator related to the Jacobian. Thus, the total absolute force for the two involved limbs can be defined as the sum of the two contributions as follows:

$$||f_C||_{l_i} = ||f_C||_{\Omega_{l_i}} + ||f_C||_{J_{l_i}} \tag{23}$$

These numbers are always positive because of the premise that only below the limits are they computed, so $e_\Omega > 0, e_J > 0$. Hence, the force $\vec{f_C}$, gets updated as:

$$\vec{f_C}(\vec{l}(1)) = d_1||f_C||_{l_1}, \qquad \vec{f_C}(\vec{l}(2)) = d_2||f_C||_{l_2} \tag{24}$$

while the other terms of $\vec{f_C}$ remain unchanged with respect to the previous time step. In this equation, d_1 and d_2 account for the direction (positive or negative), so their value can be $+1$ or -1 and are stacked in a vector $\vec{d}$. There are four possible choices for $\vec{d}$: $[+1,+1], [+1,-1], [-1,+1]$ and $[-1,-1]$. To choose the best one, the four subsequent responses are calculated by virtually applying the four possible forces $\vec{f_C}$ to the DMP and choosing the preferred directions for the actual execution such that:

1) The new reference position lies within the range of the actuators and, if so,
2) The value of Ω_{min} is the highest among the options, meaning that the chosen direction is the one that most helps the robot get out of the singular position.

The system's behavior after getting out of the singularity remains to be clarified. The designed approach involves canceling the proportional and derivative forces (since they would tend to get back to the singularity) but keeping the integrators active while they discharge gradually (since the tracking errors of equations (19) or (21) are negative in this phase) and set the scalar forces equal to the integral action to avoid abrupt changes:

$$\begin{aligned} ||f_C||_{\Omega_{out_\eta}} &= K_i[\int e_\Omega dt]_\eta \\ ||f_C||_{J_{out_\eta}} &= K_i[\int e_J dt]_\eta \end{aligned} \tag{25}$$

Equation (25) provides satisfactory results as long as the integrators are bounded below by 0, so when they are discharged, they do not try to pull the robot back towards the singularity. In other words, when they reach 0, they stop the integration process until a new singular position arises.

Figure 2 represents the scheme of the singularity evader with a DMP designed in joint coordinates and the definition of the coupling terms based on measures from a vision system, and a joint position controller (corresponding to a PD+G controller) applied directly to the output of the DMP.

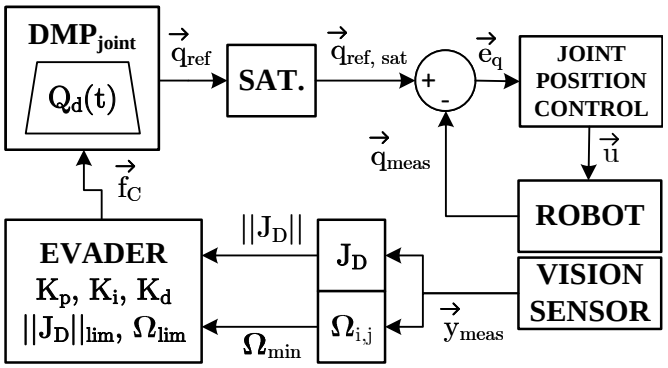

Fig. 2. DMP-embedded singularity evader in joint space based on PID control for the evasion task and low-level PD+G position control.

In [19], a method was proposed to release a robot from an initial singular position using Ω_{min} and $||J_D||$ by moving the two actuators that mostly participate in the singularity. However, that algorithm is not meant for evasion, and it relies on directly manipulating the reference position rather than providing a dynamical behavior to the system. The DMP described in this study provides a more compliant response for the robot.

The decision of choosing a controller to avoid a singularity rather than an exponential coupling action like the ones proposed for obstacle avoidance (for example, in [28], [42]) is justified by the fact that a clear reference can be established for tracking control (Ω_{lim} and $||J_D||_{lim}$), providing a more guided solution.

VI. Combined system for control

So far, it has been shown how to get the desired admittance behavior (Section IV) and the singularity avoidance (Section V) independently. In this section, the combination of both ideas is addressed. However, there are a few issues to consider before designing the whole system.

First of all, it would be desirable to have just one DMP sending out a unique reference to be tracked by the position controller. The DMP would be affected, thus, by two coupling terms corresponding to each task. This poses the dilemma of which coordinates should be chosen for the DMP. The cartesian coordinates are better suited for the admittance model because the forces are collected with a sensor in those coordinates. However, the singularity evader works at the joint level since only a pair of selected limbs are driven by its coupling action, so the DMP was defined in joint coordinates in Section V-B. For the combined task of simultaneus admittance behavior and Type II singularity avoidance, we propose a DMP in joint coordinates, and the justification will become clear in the following.

Here, we use a property described in Appendix B which states that if a DMP is identically defined for all DOFs (they all share the same dynamics), then there is a direct relationship between a coupling force exerted in cartesian coordinates ($\vec{f}_{C_y}$) and in joint coordinates ($\vec{f}_{C_q}$) using the forward and inverse Jacobian matrices as follows:

$$\vec{f}_{C_q} = J_I^{-1} \cdot J_D \cdot \vec{f}_{C_y} \tag{26}$$

This expression can be used to define the admittance behavior of a DMP in joint coordinates by feeding $\vec{f}_{C_q}$ to such DMP. In addition, J_D is a matrix already calculated since its determinant takes part in the evasion layer. Therefore, the coupling term for the admittance behavior in a DMP defined in joint coordinates could be defined as:

$$\vec{f}_{C_{adm}} = J_I^{-1} \cdot J_D \cdot \vec{F}_H \tag{27}$$

where $\vec{F}_H$ could be initially set as $\vec{F}_H = \vec{e}_F = \vec{F}_{ref} - \vec{F}_{meas}$ with $\vec{F}_{ref}$ and $\vec{F}_{meas}$ defined in cartesian coordinates as happened in Section IV.

However, a second issue arises when comparing the desired dynamic behavior of both tasks. The response of the admittance model should rather be slow to perform smooth movements in the presence of external forces (which, in the context of rehabilitation, could come from an injured human limb). However, it is crucial for the evader to get the robot out of the singularity as soon as possible, which means that a smaller t_s is likely to be chosen for the evasion task.

The adopted solution consists of the definition of a DMP suitable for evasion, with fast dynamics compared to the desired admittance model, and feed the cartesian force to designed transfer functions $H_\lambda(s)$ (one for each DOF) before multiplying by the Jacobian J_D. These transfer functions are new second-order filters comprising the desired dynamics of the admittance model and imply that the elements of the vector $\vec{F}_H$ should be defined as:

$$F_{H_\lambda}(s) = H_\lambda(s) \cdot e_{F_\lambda}(s) \tag{28}$$

H_λ allows defining a different behavior for each DOF in the cartesian space by choosing desired gains (G_{adm_λ}) and settling times (T_{adm_λ}) accordingly and applying equation (8) to obtain the constants. However, some care must be taken not to conflict with the evader's behavior, which is considered to be designed equally for all the joints and defined by the DMP parameters K_{DMP}, M_{DMP}, and D_{DMP}:

1) By choosing slower dynamics for the admittance model, the transfer functions H_λ dynamically dominate the DMP because the poles of the latter are significantly closer to the origin, so the overall system will behave as a second-order dynamical system in the presence of an external force.
2) The gain must be chosen so that the overall static gain of the system for the admittance (G_{adm_λ}) is the product of the static gain of the DMP (G_{DMP}) and that of

the transfer function (G_{H_λ}), meaning that the transfer function H_λ is defined as follows:

$$K_{H_\lambda} = \frac{G_{adm_\lambda}}{G_{DMP}},\ D_{H_\lambda} = \frac{t_{s_{adm_\lambda}} K_{H_\lambda}}{2},\ M_{H_\lambda} = \frac{D_{H_\lambda}^2}{4K_{H_\lambda}} \quad (29)$$

Thus, the general workflow for the combined system is the following:

1) Define the desired behavior of the evader with $t_{s_{eva}}$ and G_{eva}, supposed uniform for all robot limbs, and obtain the DMP constants using equation (8).
2) Define the desired behavior of the admittance model, which can differ for each cartesian coordinate, encoded in $\vec{t}_{s_{adm}}$ and $\vec{G}_{adm}$ (with $t_{s_{adm_\lambda}} >> t_{s_{eva}}$). Obtain the transfer functions H_λ using equation (29).
3) Set the constants of the goals Ω_{lim} and $||J_D||_{lim}$, which are obtained empirically, and the PID constants K_p, K_d, and K_i for singularity avoidance.
4) In execution, the $\vec{f}_{C_{eva}}$ is directly calculated using equation (24). The value $\vec{f}_{C_{adm}}$ is obtained using equations (27) and (28). The sum of both coupling actions is the total fed to the DMP:

$$\vec{f}_C = \vec{f}_{C_{eva}} + \vec{f}_{C_{adm}} \quad (30)$$

In addition, when the robot enters a singularity due to the external force, it is convenient to temporarily deactivate the admittance model, since an arbitrarily high force could beat the evader's repulsive coupling action and lead to destabilization. For that reason, as soon as either Ω_{min} or $||J_D||$ fall below their limit, a boolean pin ($sing\_pin$) deactivates and the input to the transfer function $\vec{e}'_F = \vec{e}_F \cdot sing\_pin$ holds the value $\vec{0}$. This is preferable compared to directly setting $\vec{f}_{C_{adm}}$ to $\vec{0}$ since the former implies a gentle reduction of the effect of the admittance model thanks to the effect of $H_\lambda(s)$ rather than the abrupt deactivation that would be caused with the latter option, resulting in a more compliant response.

Fig. 3 represents the scheme of the combined control system with the DMP designed in joint coordinates, the evasion and admittance modules, and the core PD+G controller applied to the output of the DMP.

As a final clarification, this scheme solves two problems at once:

1) The two objectives are expressed in different coordinate systems (end-effector cartesian coordinates for admittance control and joint coordinates for evasion), which is solved using the mapping of Appendix B and equations (26)-(27).
2) The desired dynamic behavior is also different for both objectives, which is solved by choosing the evasion for the base DMP and the admittance behavior is achieved with the adaptation of equation (28).

VII. Experiments

A. Experimental setup

1) 4-DOF PR for knee rehabilitation: The described control architecture has been tested in a knee rehabilitation PR. Knee rehabilitation requires knee flexion-extension and internal-external rotation, and hip flexion [50]. To this end, a non-redundant 4-DOF PR has been designed at the Universitat Politècnica de València [51]. Its four DOFs comprise two translational movements (x_m, z_m) in the tibiofemoral plane, one rotation (ψ) around the coronal plane, and one rotation (θ) around the tibiofemoral plane (Fig. 4a). These design specifications were established according to the analysis of the movements needed for rehabilitation after surgery and the kind of tests used for diagnosis, such as the Lachman test [52] and the pivot shift test [53].

The architecture of the 4-DOF PR is 3UPS+RPU, meaning that the mobile platform is connected to the fixed platform through three external limbs in UPS configuration and a central limb in RPU configuration, where the letters R, P, U, and S stand for the revolute, prismatic, universal, and spherical joints, respectively, and the underlined format indicate the actuated joints. This architecture provides the PR with four major advantages: a) it allows the required mobility, b) it was simple to manufacture and assemble, c) geometric tolerances

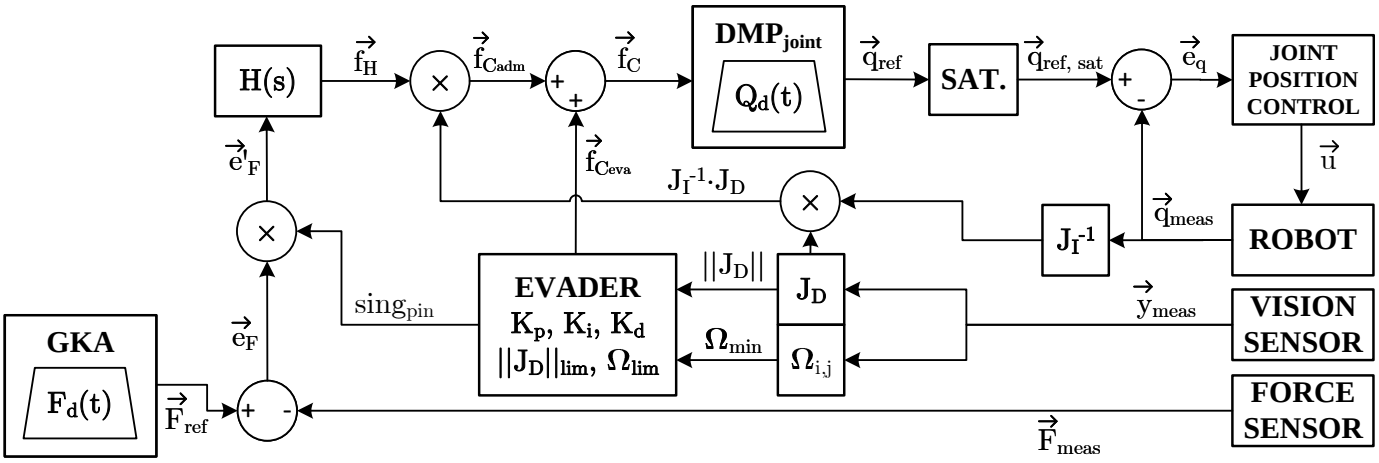

Fig. 3. DMP-embedded combined admittance control and singularity evasion in joint space by adaptation of coupling actions and low-level PD+G joint position control.

do not generate instability of the mechanism or high friction, and d) it is low cost.

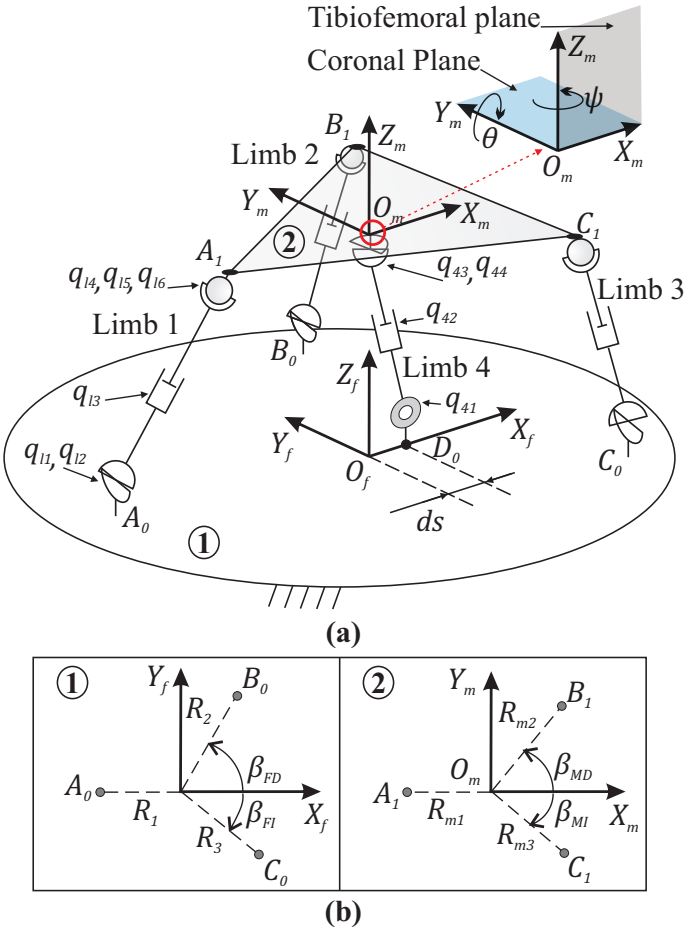

Fig. 4. Schematic (a) view and (b) configuration of the 4-DOF PR

The PR is characterized by fifteen generalized coordinates ($\vec{q}$):

$$\vec{q} = [\vec{q}_s, \vec{q}_{ind}]^T \tag{31}$$

where $\vec{q}_{ind}$ is the vector of actuated (prismatic) coordinates and $\vec{q}_s$ are the secondary coordinates, defined as:

$$\vec{q}_{ind} = [q_{13}, q_{23}, q_{33}, q_{42}]^T \tag{32}$$

$$\vec{q}_s = [q_{11}, q_{12}, q_{21}, q_{22}, q_{31}, q_{32}, q_{41}, x_m, z_m,\ \theta, \psi]^T \tag{33}$$

The configuration is defined by the points A_0, B_0, C_0, D_0 that link the fixed platform to the mobile platform attached in A_1, B_1, C_1, O_m with four limbs. The configuration is variable [13] and, in this study, the parameters are $R_1 = R_2 = R_3 = 0.4$ m, $\beta_{FD} = 90°$, $\beta_{FI} = 45°$, $d_s = 0.15$ m, $R_{m1} = R_{m2} = R_{m3} = 0.3$ m, $\beta_{MD} = 50°$, $\beta_{MI} = 90°$.

For more information about the forward and inverse kinematic analysis of this PR, see [54].

The external limbs of the PR are driven by prismatic FESTO DNCE 32-BS10 actuators, while the central limb is NIASA M100-F16. They are attached to Maxon 148867 DC motors commanded by ESCON 50/5 servo controllers. An industrial computer reads the encoder positions using a PCI 1784 Advantech card with 32-bit quadruple AB phase encoder counters. The control actions are sent through a 12-bit, 4-channel PCI 1720 Advantech card. The controllers are implemented in the industrial computer in a modular way, using Robot Operating System 2 (ROS2) [55] and the C++ programming language. A PD+G control law has been chosen for position control.

2) Vision system for pose measurement: As explained in Section V, it is preferable to use external devices to measure the cartesian pose of the robot rather than apply the forward kinematic model to the joint positions from the encoder because that model is no longer valid in the vicinity of a singularity. In this study, a 3D tracking system (3DTS) is used for this purpose, composed of 10 infrared cameras (Flex 13) manufactured by OptiTrack, with an average accuracy greater than 0.1 mm and a resolution of 1.3 Megapixels at 120 Hz. What the 3DTS actually tracks is a set of markers (reflective spheres) placed on both the fixed and the mobile platforms. Fig. 5 shows a view of the placement of the cameras and a detail of the markers.

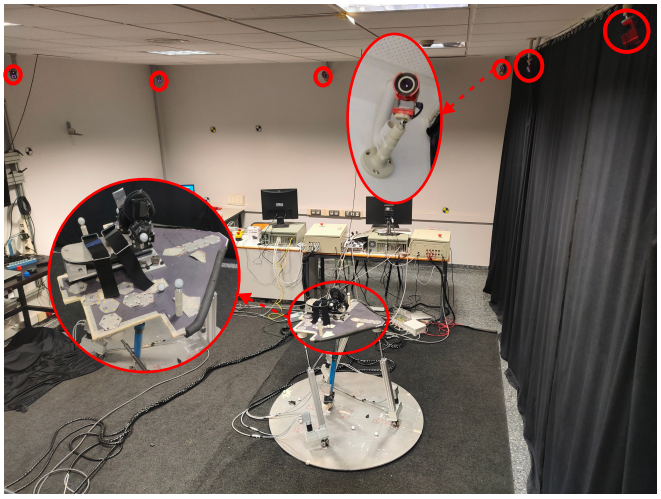

Fig. 5. OptiTrack 3D tracking system layout.

The software Motive processes those markers' locations, and that information can be collected by the industrial PC thanks to the NatNet software development kit (NatNet SDK), which allows Motive to live stream the data via UDP/multicast. A calibration process is required prior to the experiments to ensure a correct reconstruction of the 3D location of the markers.

In [18], a more detailed explanation of the 3DTS and the calibration procedure is available.

3) Force sensor: To realize the admittance behavior, a force sensor is needed to measure the interaction between the patient and the robot. In this study, the exerted forces and moments on the mobile platform from the patient's foot are measured with an FTN-Delta sensor manufactured by Schunk, which provides six-axis force/torque measurements in the range of ± 330 N (F_x, F_y), ± 990 N (F_z) for force and ± 30 N·m for torque load, with a resolution of 0.065 N (F_x, F_y), 0.125 N (F_z) for force and 0.004 N·m for moment load. A Netbox

NETB performs the signal conditioning and is connected to the industrial computer with an Ethernet connection via UDP at a rate up to 7 MHz. Fig. 6 shows the architecture of the FTN-Delta sensor and the boot used to attach the patient's foot to the sensor.

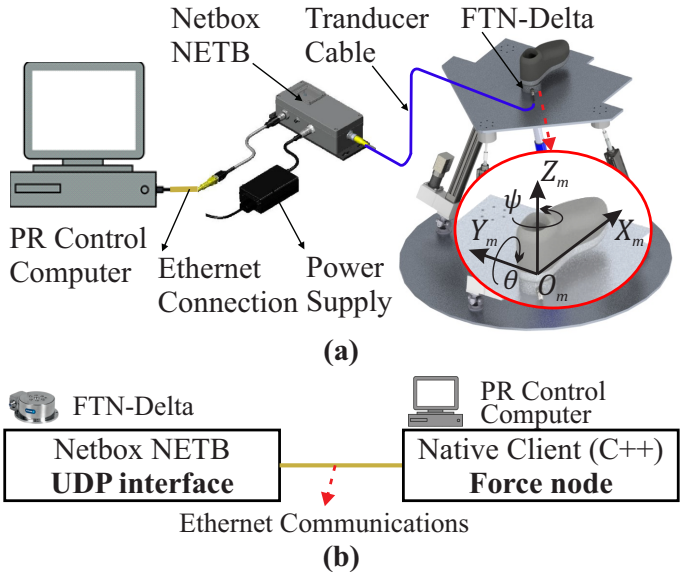

Fig. 6. FTN-Delta sensor architecture regarding (a) hardware and (b) software.

Again, a prior calibration of the sensor should be performed before the experiments to avoid sensor drifts.

B. Model specifications and test trajectories

The first step involves the selection of the parameters for both the evader and admittance models. The evader (and therefore the DMP) has been designed with a quick response of $t_{s_{eva}} = 0.2$ s and a gain of $G_{eva} = 0.001$ $\frac{\text{m}}{\text{N}}$ for the four active joints, resulting in (equation (8)) $k = 1000$ $\frac{\text{N}}{\text{m}}$, $d = 100$ $\frac{\text{Ns}}{\text{m}}$ and $m = 2.5$ kg. These values are fixed, but M, D, and K (equation (9)) are calculated at the beginning of each experiment since they are affected by the variable length of the trajectory τ. The values of Ω_{lim} and $||J_D||_{lim}$ are defined through empirical experimentation [18] and set to 2° and 0.015, respectively, and $J_I = I_{4\times4}$.

Regarding the admittance model, preferences are different for each axis, and the following vectors have been designed for good performance: $\vec{G}_{adm} = [0.004\ \frac{\text{m}}{\text{N}},\ 0.002\ \frac{\text{m}}{\text{N}},\ 0.04\ \frac{\text{rad}}{\text{N·m}},\ 0.04\ \frac{\text{rad}}{\text{N·m}}]^T$, $\vec{t}_{s_{adm}} = [4, 2, 4, 4]^T$ s. The four transfer functions H_λ are obtained using equation (29). The four TWSs $\hat{\$}_T$ for this PR are calculated as:

$$\hat{\$}_{T_1} = \begin{bmatrix} \vec{z}_{12} \\ \vec{r}_{O_m A_1} \times \vec{z}_{12} \end{bmatrix}, \hat{\$}_{T_2} = \begin{bmatrix} \vec{z}_{22} \\ \vec{r}_{O_m B_1} \times \vec{z}_{22} \end{bmatrix}, \\ \hat{\$}_{T_3} = \begin{bmatrix} \vec{z}_{32} \\ \vec{r}_{O_m C_1} \times \vec{z}_{32} \end{bmatrix}, \hat{\$}_{T_4} = \begin{bmatrix} \vec{z}_{41} \\ \vec{0} \end{bmatrix} \tag{34}$$

Two different trajectories have been designed for the evaluation. The first trajectory (*T1*) involves a hip flexion whose end pose falls in a singularity in $x_m = 0.01$ m, $z_m = 0.7$ m, $\theta = 0.15$ rad, $\psi = 0.31$ rad. The velocity to reach that pose is 0.02 $\frac{\text{m}}{\text{s}}$ for the translational DOFs and 0.03 $\frac{\text{rad}}{\text{s}}$ for the rotational ones. This trajectory is not perturbed by any external force, so the admittance model does not have any effect. This test serves to check the evader in isolation and has been used as a baseline to tune the values of K_p, K_d, and K_i of the DMP controller (see Section V), which are set to 5, 0.1, and 10, respectively.

The second trajectory (*T2*) consists of a static trajectory in position ($x_m = 0.05$ m, $z_m = 0.73$ m, $\theta = 0.07$ rad, $\psi = -0.02$ rad) with zero force references. According to the admittance model, a nonzero external force provokes robot motion, and specifically, a knee rotation in terms of a positive spin around ψ may lead the robot to a singular position.

Both trajectories are executed on the actual PR, and a comparison is established between the activation and deactivation of the evader in the presence of an external force.

C. Results and evaluation

1) Results of Trajectory 1: Fig. 7 shows the variation in position caused by the evader force on limbs 3 and 4 for *T1*. These are the limbs most affected by the singularity, i.e., $\Omega_{min} = \Omega_{34}$. This is a specific case in which the responsible limbs do not change over time in a singular region, so the algorithm simplifies since only two limbs have nonzero coupling action and they share the same integrator and repulsion force (in the scalar form). It can be deduced that the (avoided) singular configuration starts at approximately $t = 15$ s and ends at $t = 36$ s. The deviation of the actual position with respect to the original reference (the one fed to the DMP) is $\Delta q = 4$ mm. This value is the same for both limbs since the dynamics and PID constants for the evader have been chosen uniformly for all the active joints. However, it is a positive increment for limb 3 and negative for limb 4, so $\vec{d} = [+1, -1]$ (defined after trying the four possibilities in each time step, see Section V-B).

The profile of the coupling actions that lead to these results is depicted in Fig. 8. They are the sum of the proportional, derivative, and integral components. Although these coupling forces are designed abstractly (are applied to a virtual mass-spring-damper), the units (N) have been defined by analogy to a real system.

To know which singularity indicator caused the activation of the evader mechanism, Fig. 9 shows the values of both $||J_D||$ and Ω_{min} with their corresponding limits.

The most restrictive indicator for this experiment is Ω_{min} since the trajectory tries to fall below its limit at $t = 15$ s, activating the coupling term. It can be seen how this signal converges to its limit rather than falling toward 0, thanks to the effect of the PID and the resulting coupling force of Fig. 8. The initial stage below the limit occurs because the integral component of the PID needs to charge, and it corresponds to the gradual increase of the coupling force from $t = 15$ s in Fig. 8. In the same way, the connection back to the original trajectory after the singular configuration is also gradual, while the integrator discharges to its clipped value of 0. This coupling force can be seen as a repulsive force similar to that

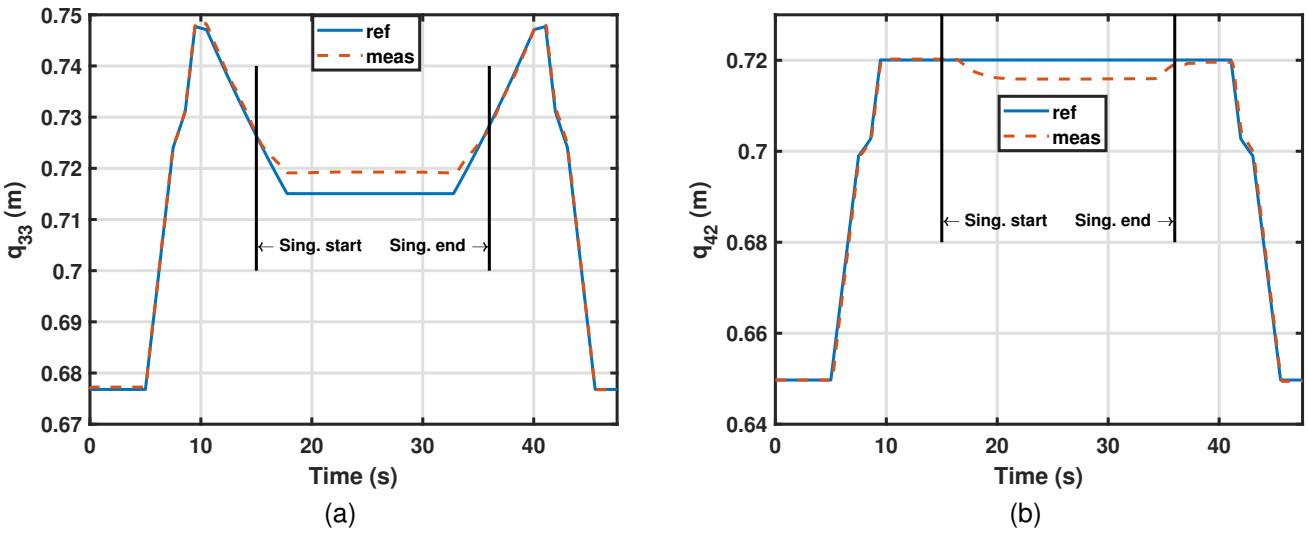

Fig. 7. Original reference and actual positions of limbs (a) 3, and (b) 4, during the execution of *T1*.

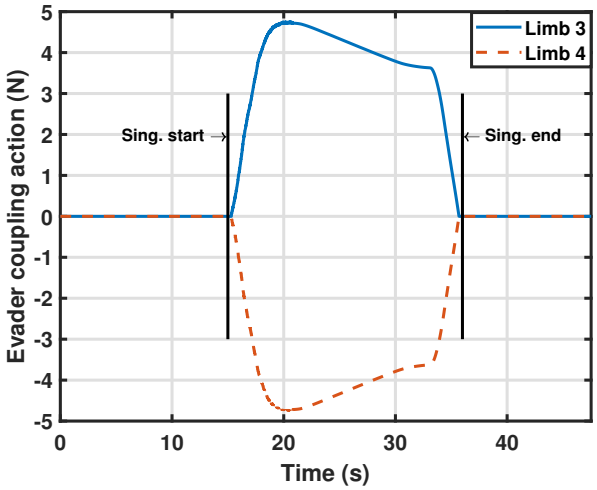

Fig. 8. Overall evader forces applied during the execution of *T1*.

applied in obstacle avoidance with DMPs; however, having an objective control like the one proposed in this study offers a more guided solution which becomes of paramount importance in physical human-robot interaction settings like rehabilitation. A recording of this experiment is available in: *http://roboprop.ai2.upv.es/wp-content/uploads/2022/10/dmp_evasor_TRR15_vf.mp4*.

2) Results of Trajectory 2: In the experiment with *T1*, the deactivation of the evader might not have a significant impact as long as the applied external force becomes zero, which was fulfilled during the first test but does not occur in a realistic human-robot interaction setup. In the following experiment with *T2*, we further justify the statement that in a Type II singular configuration, the PR cannot bear external forces, and therefore, we also show the actual utility of the evader. The admittance module is active for this experiment with a static reference position, and an external torque is applied around ψ to lead the robot to a singularity.

Figure 10 shows the value of ψ for the experiments both with and without the evader activation, and Fig. 11 depicts the torque in Z exerted on the PR in those experiments.

The first important fact to note is that the experiment without the evader was stopped soon after its start because the PR underwent a singular configuration and became unstable due to the unbearable external force. However, the PR in the experiment with the evader was kept stable and off the singular configuration thanks to the evader action. From Fig. 10, it can be deduced that the singularity starts beyond $\psi = 0.2$ rad approximately.

On the other hand, Fig. 11 proves that even exerting a greater force in the experiment with the evader (which reaches 20 N·m) does not turn the system unstable, in constrast to the experiment without the evader, where a smaller force suffices to destabilize the system.

No matter how hard the patient tries to push the robot toward the singularity (considering reasonably high forces for a healthy human leg), the combined effect of the deactivation of the admittance model and the evader contribution through its coupling force can keep the PR in safe positions.

Furthermore, the deactivation of the admittance model within a singularity is gradual, so the patient does not feel an abrupt force or movement, but it is instead a struggle between the human and the robot. This effect can be seen in Figure 12, where the indicator Ω_{min} is plotted, which is again the most restrictive, so $||J_D||$ values are omitted. In this experiment, the affected limbs are again 3 and 4. From approximately $t = 30$ s, the wiggly blue curve represents this struggle when the evader is activated to push the PR in the opposite direction to that of the human force. This effect is visibly smooth and slight, making it convenient for rehabilitation tasks. To appreciate this, a video of this experiment can be visited through this URL: *http://roboprop.ai2.upv.es/wp-content/uploads/2022/10/dmp_c*

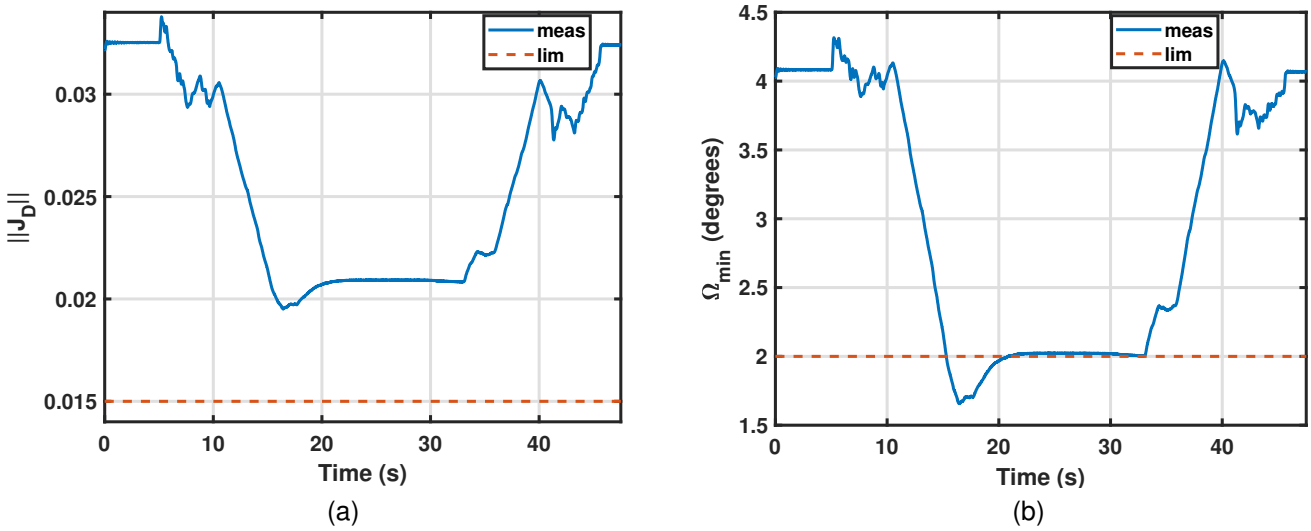

Fig. 9. Indicators of singularity (a) $||J_D||$, (b) Ω_{min} for experiment *T1*.

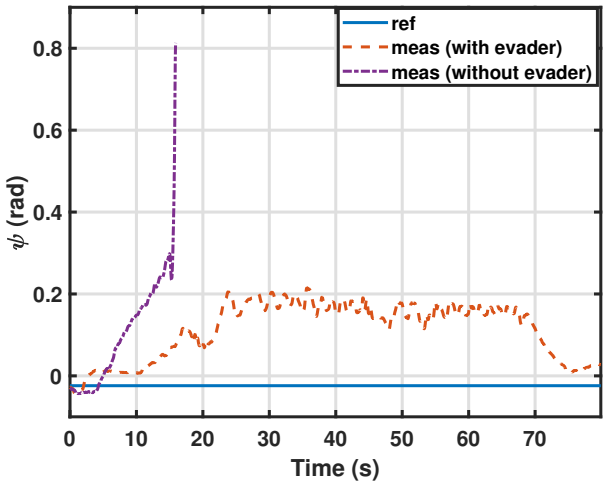

Fig. 10. Original reference and actual ψ for experiment *T2* with and without evader.

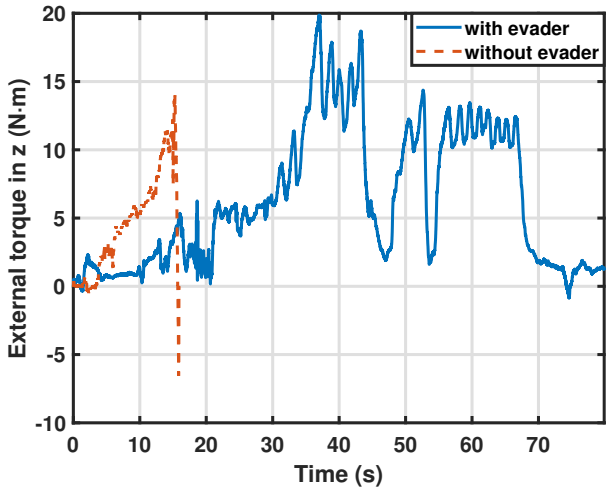

Fig. 11. External torque in z M_z for the experiment *T2* with and without evader.

on_evasor_vf.mp4.

Figure 12 also depicts why the system without evader was destabilized: the value of Ω_{min} reached 0 right before diverging, bringing to light the utility of the indicator Ω_{min} for singularity detection. It is also important to highlight that the thresholds Ω_{lim} and $||J_D||_{lim}$ are not boundaries that separate trajectories totally clear of singularities from extremely dangerous zones because singular configurations are gradually reached and the indicators, empirically obtained, may be different among them. The values used here are a good tradeoff, and certain exceedance in controlled environments (as occurs in Fig 9b and Fig 12) should not be worrying. The video in the following URL shows the behavior when the evader is not activated: *http://roboprop.ai2.upv.es/wp-content/uploads/2022/10/dmp_sin_evasor_vf.mp4*.

In Fig. 13, the admittance (13a) and evader (13b) coupling actions for limbs 3 and 4 are represented. The profile of the admittance coupling action (in joint space) is another proof that the deactivation is gradual since the values do not directly drop to 0 (this becomes clearer for limb 3) but rather decrease gradually as the evader also acts, until the PR gets released and the human-robot interaction continues. The evader is able to keep this interaction compliant thanks to the effect of the integral component, which causes the force to remain stable even in a state of continuous fluctuation of singularity crossing, as happens in this experiment.

VIII. Conclusion

In this paper, a new insight into the DMP has been provided from two perspectives: i) the capability to define the dynamic behavior of the DMP by choosing the proper constants of the

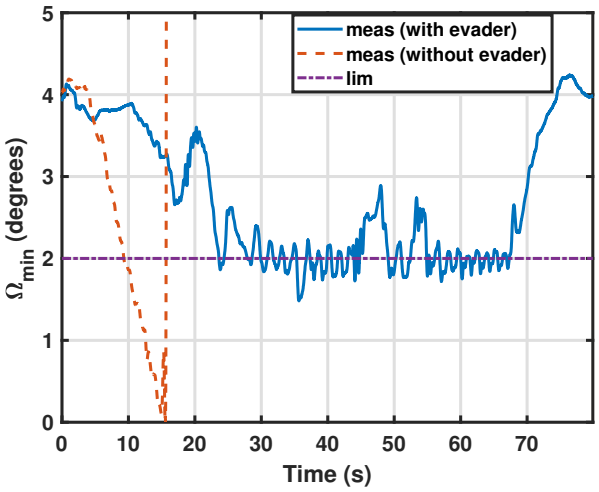

Fig. 12. Values of Ω_{min} for the experiment *T2* with and without the evader.

mass-spring-damper system, which has been extended from the more simple and traditional spring-damper system with no other constraint than the critically damped response, and ii) the possibility to introduce objective controls in the system and embed them inside the coupling actions through a control law. A new algorithm for Type II singularity avoidance has also been presented, which precisely defines an objective on the DMP and implies a step forward in the discipline of safe human-robot interaction.

These goals have been successfully fulfilled through an experiment with a 3UPS+RPU PR meant for knee rehabilitation, where two different tasks were performed simultaneously: admittance behavior and singularity avoidance. The admittance model has been embedded into the DMP thanks to the Gaussian Kernel Approximators learned for the force trajectory and the phase sharing. The experiment showed that a raw admittance controller is unsafe for human-robot interaction since it can drive the robot toward unstable singular positions. Therefore, the inclusion of the designed evader plays a significant role, at the expense of the extra instrumentation needed to measure the robot's pose. Nevertheless, this combination is not trivial since the two tasks are not naturally expressed in the same coordinate system, nor do they share the desired dynamic response, so we have also addressed how to adapt both issues.

Besides, the singularity evader only uses the two limbs more involved in the singularity given by the measurement of Ω_{min}, so the deviation is tiny, as shown in the experiment of the evader in isolation (for which a deviation of 4 mm is enough). When combined with the admittance model, the evader performs smooth deactivations of the admittance behavior, which do not cause the loss of the compliant manipulation or an abrupt change uncomfortable for the patient. The evader is also applicable to any PR prone to undergoing Type II singular configurations, so our method generalizes to a wide range of applications.

Type II singularities are exclusive of PRs; however, the developed methodology based on establishing objective controls embedded in a DMP and designing the coupling actions to accomplish such goals can be applied to a serial robot whose task can be characterized in such a way (for example, in an obstacle avoidance task).

This study opens up new possible lines of work. The adaptation is performed during the evasion stage via a PID controller, however, all the parameters (the DMP, admittance transfer functions and controllers) are kept constant during the experiment, so in future work, some of these variables can be modified online for further adaptation. Also, methods like iterative learning control (ILC) are interesting since rehabilitation usually involves the repetition of the same experiment. In this context of rehabilitation, it is also convenient to compare trajectories for diagnosis, and the DMP encodes the trajectories in such a way that facilitates this task by means of the learned weights. The proposed formulation could also benefit from that feature, as well as the analysis of the coupling actions for the reproduction of trajectories and imitation learning.

APPENDIX A
DYNAMIC PARAMETERS OF SECOND-ORDER SYSTEM TO FULFILL CONSTRAINTS

In the following, we derive the solutions of k, d, and m from equation (8) which simultaneously fulfill the three constraints expressed in Section III-B for a standard mass-spring-damper transfer function like the expressed in (7). For the value of k, it suffices to apply the theorem of static gain, which states that a generic transfer function $TF(s)$ has a gain in steady state equal to $G = TF(0)$, and in this case $TF(0) = \frac{1}{k}$, so $k = \frac{1}{G}$.

The critically damped behavior (constraint 3) is obtained if the transfer function has two equal poles (or a single pole of multiplicity 2). For this study, we express the transfer function as a standard second-order system:

$$TF(s) = \frac{K_{TF}\omega_n^2}{s^2 + 2\xi\omega_n s + \omega_n^2} \tag{35}$$

where K_{TF} is the gain, ω_n is the natural frequency, and ξ is the damping factor. By comparing the transfer functions of equations (35) and (7), the values of K_{TF}, ω_n, and ξ are calculated as:

$$K_{TF} = \frac{1}{k} \quad \omega_n = \sqrt{\frac{k}{m}} \quad \xi = \frac{d}{2\sqrt{km}} \tag{36}$$

The poles of this system are given by:

$$p_{1,2} = -\xi\omega_n \pm \omega_n\sqrt{1-\xi^2} \tag{37}$$

If $\xi = 1$, the imaginary component disappears, so the pole of multiplicity two is $-\omega_n$. This is the condition for the critically damped behavior, and making $\xi = 1$, from equation (36) we obtain:

$$d^2 = 4km \tag{38}$$

The last constraint is the settling time, and since there is one real pole, the settling time with the criterion of 98% of the final value is:

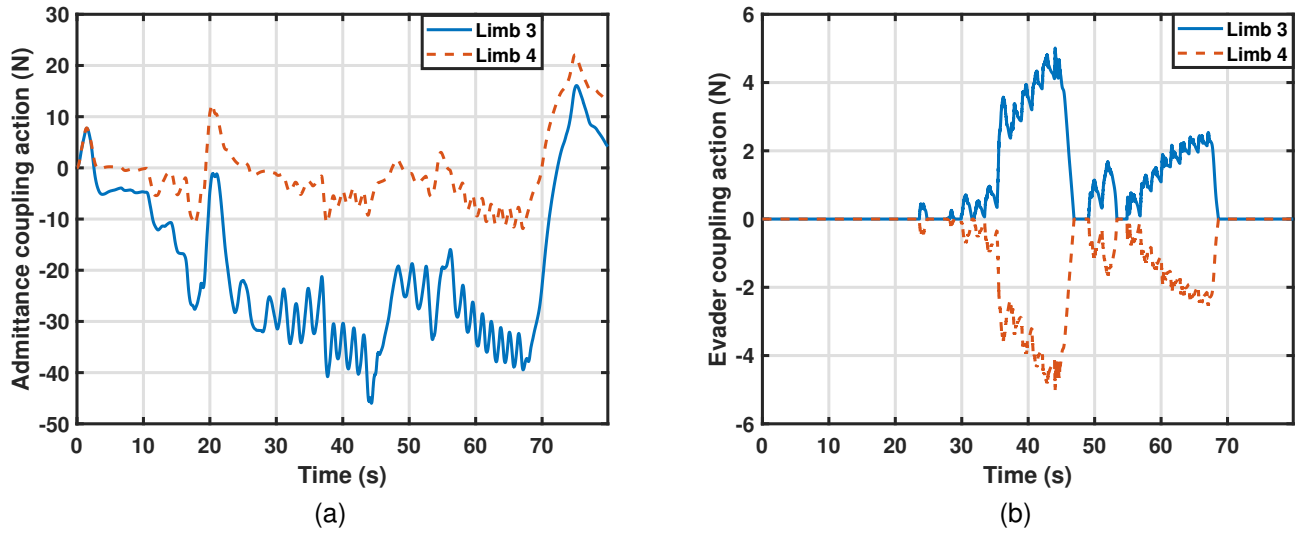

Fig. 13. Coupling actions by (a) admittance model, and (b) evader for limbs 3 and 4 in the experiment *T2*.

$$t_s = \frac{4}{\omega_n} = 4\sqrt{\frac{m}{k}} \tag{39}$$

Substituting the value of m from equation (38) in (39), the result is:

$$t_s = 4\sqrt{\frac{d^2}{4k^2}} = 2\frac{d}{k} \tag{40}$$

The value of d is obtained with equation (40), and afterward the value of m is calculated with (38), obtaining the sought expressions of equation (8).

Appendix B
Coupling action conversion from cartesian to joint coordinates

Next, the demonstration of the coupling action conversion (equation (26)) is presented starting from the differential kinematics equation (15) and assuming that the encoded DMP is identical for all DOFs, i.e., they share the constants M, D, and K. We want to show that the response of a DMP defined in cartesian space can be emulated with a DMP defined in joint space, and obtain the expression that fulfills this match.

In Fig. 14, this problem is posed graphically, where the mapping from $\vec{f}_{C_y}$ to $\vec{f}_{C_q}$, denoted by A, is the matrix to obtain. If the natural flow of the phase of the DMP is not altered with any of its capabilities (for example, the variation of velocity or the phase stopping), this mechanism is equivalent to a linear system given by its transfer functions $DMP_1(s) = DMP_2(s) = \cdots = DMP_\Lambda(s)$ which calculate a variation $(\overrightarrow{\Delta y}, \overrightarrow{\Delta q})$ to sum to the original references $(\vec{y}_d, \vec{q}_d)$ to obtain the final references $(\vec{y}_{ref}, \vec{q}_{ref})$.

The following expression must be fulfilled to prove the equality between both responses:

$$\vec{q}_{ref} = IK(\vec{y}_{ref}) \tag{41}$$

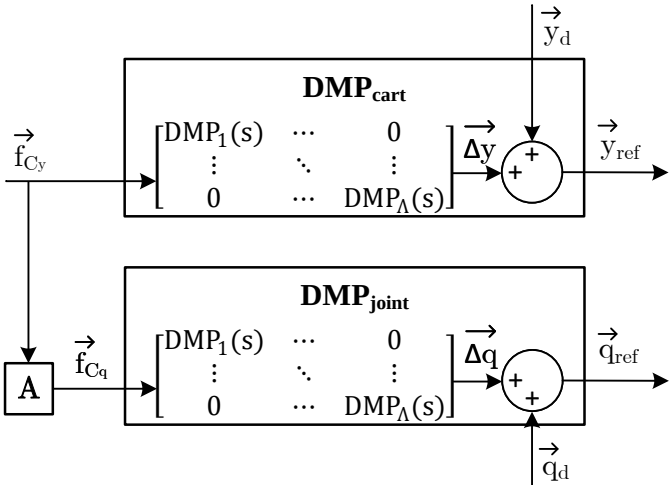

Fig. 14. Graphical representation of the equivalence of responses using a DMP defined in cartesian and joint space.

where $IK(\cdot)$ is the inverse kinematics operator. Beforehand, we assume that the original references do fulfill that expresion: $\vec{q}_d = IK(\vec{y}_d)$. Moreover, the matrices $DMP_{cart} = DMP_{joint}$ are equal, both diagonal with the same values in the diagonal. Following the upper branch, the relationship between $\vec{y}_{ref}$ and $\vec{f}_{C_y}$ is the following:

$$\vec{y}_{ref} = \vec{y}_d + \overrightarrow{\Delta y} = \vec{y}_d + DMP_{cart} \cdot \vec{f}_{C_y} \tag{42}$$

On the other hand, the following applies to the lower branch:

$$\vec{q}_{ref} = \vec{q}_d + \overrightarrow{\Delta q} = IK(\vec{y}_d) + DMP_{joint} \cdot \vec{f}_{C_q} \tag{43}$$

We now want to obtain $IK(\vec{y}_{ref})$, and the following statement can be applied:

$$IK(\vec{y}_d + \overrightarrow{\Delta y}) \approx IK(\vec{y}_d) + \overrightarrow{\Delta q} \tag{44}$$

This approximation gets more valid as the displacement $\overrightarrow{\Delta y}$ gets smaller since the $IK(\cdot)$ operator becomes more linear. This happens as the sampling time is reduced and the changes get smoother (which is accomplished thanks to the transfer functions), and equation (15) can also be applied in this situation for a slight increment, resulting in:

$$\overrightarrow{\Delta q} \approx J_I^{-1} \cdot J_D \cdot \overrightarrow{\Delta y} \tag{45}$$

Now, we can apply equations (44) and (45) to (42) to obtain:

$$IK(\vec{y}_{ref}) \approx IK(\vec{y}_d) + J_I^{-1} \cdot J_D \cdot DMP_{cart} \cdot \vec{f}_{C_y} \tag{46}$$

In order to fulfill equation (41), the expressions (43) and (46) must match, and this is achieved if:

$$DMP_{joint} \cdot \vec{f}_{C_q} = J_I^{-1} \cdot J_D \cdot DMP_{cart} \cdot \vec{f}_{C_y} \tag{47}$$

Finally, we used the two properties mentioned above:

1) Both cartesian and joint DMP matrices are identical: $DMP_{cart} = DMP_{joint}$.
2) They are diagonal, and all the members of the diagonal are the same: $DMP_1(s) = DMP_2(s) = \cdots = DMP_\Lambda(s)$.

The second property allows the second term of Equation (47) to commute with respect to DMP_{cart}, so it can be placed at the beginning of the expression without altering the result. Afterward, the matrices of DMP_{joint} and DMP_{cart} can be removed thanks to the first property, leaving:

$$\vec{f}_{C_q} = J_I^{-1} \cdot J_D \cdot \vec{f}_{C_y} \tag{48}$$

This was the intended result of the expression (26), and it entails the following mapping A:

$$A = J_I^{-1} \cdot J_D \tag{49}$$

This result indicates that if some desired behavior has been designed for a DMP in cartesian coordinates (encoded in DMP_{cart}), and as long as all the DOFs share the dynamics, it can be extrapolated to the joint space just by defining the same DMP in joint coordinates and mapping the coupling action using (48). Of course, this can be applied in the opposite direction to obtain a behavior in cartesian coordinates from that in joint coordinates by solving (48) for $\vec{f}_{C_y}$.

The result also states that the mapping for the coupling action is the same as the one used for the velocities (equation (15)), which seems counterintuitive since the conversion between forces involves the transpose Jacobian according to the principle of virtual power. However, these are not real but virtual forces applied on a virtual system with the aim of outputting desired positions and velocities. For this reason, the analysis showed that the kinematic relationship should be applied instead.

Lastly, the approximations of equations (44)-(46) depend on the sample time and the speed of the transfer functions. In all the experiments performed, with a sample time of 0.01 s, the response is very accurate as seen in the experimental results.

REFERENCES

[1] C. Bartneck, T. Belpaeme, F. Eyssel, T. Kanda, M. Keijsers, and S. Šabanović, *Human-Robot Interaction: An Introduction*. Cambridge University Press, 2020.

[2] S. Xie, "Advanced robotics for medical rehabilitation," *Springer tracts in advanced robotics*, vol. 108, no. 1, p. 357, 2016.

[3] Y. Patel and P. George, "Parallel Manipulators Applications—A Survey," *Modern Mechanical Engineering*, vol. 2, pp. 57–64, 08 2012.

[4] S. Briot and W. Khalil, *Dynamics of Parallel Robots*. Springer, 09 2015, vol. 35.

[5] I. Díaz, J. J. Gil, and E. Sánchez, "Lower-limb robotic rehabilitation: Literature review and challenges," *Journal of Robotics*, vol. 2011, 01 2011.

[6] P. Sui, L. Yao, Z. Lin, H. Yan, and J. S. Dai, "Analysis and synthesis of ankle motion and rehabilitation robots," in *2009 IEEE International Conference on Robotics and Biomimetics (ROBIO)*, 2009, pp. 2533–2538.

[7] J. Cazalilla, M. Vallés, V. Mata, M. Díaz-Rodríguez, and A. Valera, "Adaptive control of a 3-DOF parallel manipulator considering payload handling and relevant parameter models," *Robotics and Computer-Integrated Manufacturing*, vol. 30, no. 5, pp. 468–477, Oct. 2014.

[8] A. Q. Keemink, H. van der Kooij, and A. H. Stienen, "Admittance control for physical human–robot interaction," *The International Journal of Robotics Research*, vol. 37, no. 11, pp. 1421–1444, 2018.

[9] J. A. Saglia, N. G. Tsagarakis, J. S. Dai, and D. G. Caldwell, "Control Strategies for Patient-Assisted Training Using the Ankle Rehabilitation Robot (ARBOT)," *IEEE/ASME Transactions on Mechatronics*, vol. 18, no. 6, pp. 1799–1808, 2013.

[10] W. Yang Ho, W. Kraus, A. Mangold, and A. Pott, "Haptic Interaction with a Cable-Driven Parallel Robot Using Admittance Control," in *Cable-Driven Parallel Robots*, A. Pott and T. Bruckmann, Eds. Cham: Springer International Publishing, 2015, pp. 201–212.

[11] C. Gosselin and J. Angeles, "Singularity analysis of closed-loop kinematic chains," *IEEE Transactions on Robotics and Automation*, vol. 6, no. 3, pp. 281–290, 1990.

[12] M. Slavutin, O. Shai, A. Sheffer, and Y. Reich, "A novel criterion for singularity analysis of parallel mechanisms," *Mechanism and Machine Theory*, vol. 137, pp. 459–475, 2019.

[13] C. Llopis-Albert, F. Valero, V. Mata, J. Pulloquinga, P. Zamora-Ortiz, and R. Escarabajal, "Optimal Reconfiguration of a Parallel Robot for Forward Singularities Avoidance in Rehabilitation Therapies. A Comparison via Different Optimization Methods," *Sustainability*, vol. 12, pp. 1–18, 07 2020.

[14] Y. F. Zhang, J. L. Gong, and X. T. Wei, "Singularity elimination of parallel mechanism by redundant actuations," in *Advanced Materials Research*, vol. 204. Trans Tech Publ, 2011, pp. 1540–1543.

[15] J. Gallardo, J. Rico, A. Frisoli, D. Checcacci, and M. Bergamasco, "Dynamics of parallel manipulators by means of screw theory," *Mechanism and Machine Theory*, vol. 38, no. 11, pp. 1113–1131, 2003.

[16] M. S. C. Yuan, F. Freudenstein, and L. S. Woo, "Kinematic Analysis of Spatial Mechanisms by Means of Screw Coordinates. Part 2—Analysis of Spatial Mechanisms," *Journal of Engineering for Industry*, vol. 93, no. 1, pp. 67–73, 02 1971.

[17] Y. Takeda and H. Funabashi, "Motion Transmissibility of In-Parallel Actuated Manipulators," *JSME international journal. Ser. C, Dynamics, control, robotics, design and manufacturing*, vol. 38, no. 4, pp. 749–755, 1995.

[18] J. L. Pulloquinga, V. Mata, A. Valera, P. Zamora-Ortiz, M. Díaz-Rodríguez, and I. Zambrano, "Experimental Analysis of Type II Singularities and Assembly Change Points in a 3UPS+RPU Parallel Robot," *Mechanism and Machine Theory*, vol. 158, p. 104242, 01 2021.

[19] J. L. Pulloquinga, R. J. Escarabajal, J. Ferrándiz, M. Vallés, V. Mata, and M. Urízar, "Vision-Based Hybrid Controller to Release a 4-DOF Parallel Robot from a Type II Singularity," *Sensors*, vol. 21, no. 12, 2021.

[20] S. Schaal, *Dynamic Movement Primitives -A Framework for Motor Control in Humans and Humanoid Robotics*. Tokyo: Springer Tokyo, 2006, pp. 261–280.

[21] A. J. Ijspeert, J. Nakanishi, H. Hoffmann, P. Pastor, and S. Schaal, "Dynamical movement primitives: Learning attractor models for motor behaviors," *Neural Computation*, vol. 25, no. 2, pp. 328–373, 2013.

[22] M. Saveriano, F. J. Abu-Dakka, A. Kramberger, and L. Peternel, "Dynamic movement primitives in robotics: A tutorial survey," *CoRR*, vol. abs/2102.03861, 2021.

[23] P. Pastor, M. Kalakrishnan, F. Meier, F. Stulp, J. Buchli, E. Theodorou, and S. Schaal, "From dynamic movement primitives to associative skill memories," *Robotics and Autonomous Systems*, vol. 61, no. 4, pp. 351–361, 2013, models and Technologies for Multi-modal Skill Training.

[24] F. Meier, E. Theodorou, and S. Schaal, "Movement Segmentation and Recognition for Imitation Learning," in *Proceedings of the Fifteenth International Conference on Artificial Intelligence and Statistics*, ser. Proceedings of Machine Learning Research, N. D. Lawrence and M. Girolami, Eds., vol. 22. La Palma, Canary Islands: PMLR, 21–23 Apr 2012, pp. 761–769.

[25] A. Ude, A. Gams, T. Asfour, and J. Morimoto, "Task-specific generalization of discrete and periodic dynamic movement primitives," *IEEE Transactions on Robotics*, vol. 26, no. 5, pp. 800–815, 2010.

[26] S. Schaal, P. Mohajerian, and A. Ijspeert, "Dynamics systems vs. optimal control — a unifying view," in *Computational Neuroscience: Theoretical Insights into Brain Function*, ser. Progress in Brain Research, P. Cisek, T. Drew, and J. F. Kalaska, Eds. Elsevier, 2007, vol. 165, pp. 425–445.

[27] A. Gams, B. Nemec, A. J. Ijspeert, and A. Ude, "Coupling movement primitives: Interaction with the environment and bimanual tasks," *IEEE Transactions on Robotics*, vol. 30, no. 4, pp. 816–830, 2014.

[28] H. Hoffmann, P. Pastor, D.-H. Park, and S. Schaal, "Biologically-inspired dynamical systems for movement generation: Automatic real-time goal adaptation and obstacle avoidance," in *2009 IEEE International Conference on Robotics and Automation*, 2009, pp. 2587–2592.

[29] J. L. Pulloquinga, R. J. Escarabajal, M. Vallés, Á. Valera, and V. Mata, "Trajectory Planner for Type II Singularities Avoidance Based on Output Twist Screws," in *Advances in Robot Kinematics 2022*, O. Altuzarra and A. Kecskeméthy, Eds. Cham: Springer International Publishing, 2022, pp. 445–452.

[30] D. Six, S. Briot, A. Chriette, and P. Martinet, "A Controller Avoiding Dynamic Model Degeneracy of Parallel Robots During Singularity Crossing," *Journal of Mechanisms and Robotics*, vol. 9, no. 5, 08 2017.

[31] B. Nouri Rahmat Abadi and J. A. Carretero, "Modeling and Real-Time Motion Planning of a Class of Kinematically Redundant Parallel Mechanisms With Reconfigurable Platform," *Journal of Mechanisms and Robotics*, vol. 15, no. 2, 06 2022.

[32] N. Baron, A. Philippides, and N. Rojas, "A robust geometric method of singularity avoidance for kinematically redundant planar parallel robot manipulators," *Mechanism and Machine Theory*, vol. 151, p. 103863, 2020.

[33] C. Vaida, I. Birlescu, A. Pisla, I.-M. Ulinici, D. Tarnita, G. Carbone, and D. Pisla, "Systematic design of a parallel robotic system for lower limb rehabilitation," *IEEE Access*, vol. 8, pp. 34 522–34 537, 2020.

[34] J. Wu, J. Gao, R. Song, R. Li, Y. Li, and L. Jiang, "The design and control of a 3DOF lower limb rehabilitation robot," *Mechatronics*, vol. 33, pp. 13–22, 2016.

[35] N. Hogan, "Impedance Control: An Approach to Manipulation," in *1984 American Control Conference*, 1984, pp. 304–313.

[36] D. Bristow, M. Tharayil, and A. Alleyne, "A survey of iterative learning control," *IEEE Control Systems Magazine*, vol. 26, no. 3, pp. 96–114, 2006.

[37] E. Shahriari, A. Kramberger, A. Gams, A. Ude, and S. Haddadin, "Adapting to contacts: Energy tanks and task energy for passivity-based dynamic movement primitives," in *2017 IEEE-RAS 17th International Conference on Humanoid Robotics (Humanoids)*, 2017, pp. 136–142.

[38] A. Kramberger, E. Shahriari, A. Gams, B. Nemec, A. Ude, and S. Haddadin, "Passivity based iterative learning of admittance-coupled dynamic movement primitives for interaction with changing environments," in *2018 IEEE/RSJ International Conference on Intelligent Robots and Systems (IROS)*, 2018, pp. 6023–6028.

[39] N. Wang, C. Chen, and C. Yang, "A robot learning framework based on adaptive admittance control and generalizable motion modeling with neural network controller," *Neurocomputing*, vol. 390, pp. 260–267, 2020.

[40] S. Calinon, F. Guenter, and A. Billard, "On Learning, Representing, and Generalizing a Task in a Humanoid Robot," *IEEE Transactions on Systems, Man, and Cybernetics, Part B (Cybernetics)*, vol. 37, no. 2, pp. 286–298, 2007.

[41] A. Agarwal, C. Nasa, and S. Bandyopadhyay, "Dynamic singularity avoidance for parallel manipulators using a task-priority based control scheme," *Mechanism and Machine Theory*, vol. 96, pp. 107–126, 2016.

[42] D.-H. Park, H. Hoffmann, P. Pastor, and S. Schaal, "Movement reproduction and obstacle avoidance with dynamic movement primitives and potential fields," in *Humanoids 2008 - 8th IEEE-RAS International Conference on Humanoid Robots*, 2008, pp. 91–98.

[43] P. Pastor, H. Hoffmann, T. Asfour, and S. Schaal, "Learning and generalization of motor skills by learning from demonstration," in *2009 IEEE International Conference on Robotics and Automation*, 2009, pp. 763–768.

[44] P. Pastor, L. Righetti, M. Kalakrishnan, and S. Schaal, "Online movement adaptation based on previous sensor experiences," in *2011 IEEE/RSJ International Conference on Intelligent Robots and Systems*, 2011, pp. 365–371.

[45] C. G. Atkeson, A. W. Moore, and S. Schaal, "Locally weighted learning," *Lazy learning*, pp. 11–73, 1997.

[46] M. Karlsson, A. Robertsson, and R. Johansson, "Convergence of Dynamical Movement Primitives with Temporal Coupling," in *2018 European Control Conference (ECC)*, 2018, pp. 32–39.

[47] A. Ude, B. Nemec, T. Petrić, and J. Morimoto, "Orientation in Cartesian space dynamic movement primitives," in *2014 IEEE International Conference on Robotics and Automation (ICRA)*, 2014, pp. 2997–3004.

[48] F. J. Abu-Dakka, B. Nemec, J. A. JØrgensen, T. R. Savarimuthu, N. Krüger, and A. Ude, "Adaptation of manipulation skills in physical contact with the environment to reference force profiles," *Auton. Robots*, vol. 39, no. 2, p. 199–217, aug 2015.

[49] J. Wang, C. Wu, and X.-J. Liu, "Performance evaluation of parallel manipulators: Motion/force transmissibility and its index," *Mechanism and Machine Theory*, vol. 45, no. 10, pp. 1462–1476, 2010.

[50] D. A. Neumann, "Kinesiology of the musculoskeletal system; Foundation for rehabilitation," *Mosby & Elsevier*, 2010.

[51] M. Vallés, P. Araujo-Gómez, V. Mata, A. Valera, M. Díaz-Rodríguez, Álvaro Page, and N. M. Farhat, "Mechatronic design, experimental setup, and control architecture design of a novel 4 DoF parallel manipulator," *Mechanics Based Design of Structures and Machines*, vol. 46, no. 4, pp. 425–439, 2018.

[52] S. Wiertsema, H. van Hooff, L. Migchelsen, and M. Steultjens, "Reliability of the KT1000 arthrometer and the Lachman test in patients with an ACL rupture," *The Knee*, vol. 15, no. 2, pp. 107–110, 2008.

[53] N. Lopomo, S. Zaffagnini, C. Signorelli, S. Bignozzi, G. Giordano, G. M. Marcheggiani Muccioli, and A. Visani, "An original clinical methodology for non-invasive assessment of pivot-shift test," *Computer methods in biomechanics and biomedical engineering*, vol. 15, no. 12, pp. 1323–1328, 2012.

[54] P. Araujo-Gómez, V. Mata, M. Díaz-Rodríguez, n. Valera, and A. Page, "Design and Kinematic Analysis of a Novel 3UPS/RPU Parallel Kinematic Mechanism With 2T2R Motion for Knee Diagnosis and Rehabilitation Tasks," *Journal of Mechanisms and Robotics*, vol. 9, 09 2017.

[55] V. DiLuoffo, W. R. Michalson, and B. Sunar, "Robot Operating System 2: The need for a holistic security approach to robotic architectures," *International Journal of Advanced Robotic Systems*, vol. 15, no. 3, 2018.

Rafael J. Escarabajal received the B.Eng. in Industrial Engineering in 2017 and the M.Sc Degree in Automatic control and Robotics in 2019 from the Universitat Politècnica de València. Currently, he is a Ph.D. candidate in robotics and industrial computing at the Instituto Universitario de Automática e Informática Industrial, Universidad Politècnica de València. His research interests include robot learning and control, optimization, and artificial intelligence.

José L. Pulloquinga received his degree in Mechatronics Engineering in 2014 from The University of the Armed Forces-ESPE, Ecuador. He received his M.Sc Degree in Mechatronics and Robotics in 2018 from the Escuela Politécnica Nacional, Ecuador. Currently, he is a Ph.D. candidate in automatic, robotics and industrial computing from Universidad Politècnica de València, Spain. His research interests include robot control, singularities, and artificial intelligence.

Ángel Valera (Member, IEEE) received the B.Eng. in Computer Science in 1988, the M.Sc. Degree in Computer Science in 1990, and his Ph.D. in Control Engineering in 1998 from the Universitat Politècnica de València (UPV), Spain. He has been a professor of automatic control at the UPV since 1989 and now he is Full Professor at the Systems and Control Engineering Department. He has taken part in 75 research and mobility projects funded by local industries, government and European community and he has published over 190 technical papers in journals, technical conferences, and seminars. His research interests include mechatronics, industrial and mobile robots and robot control.

Vicente Mata is a Mechanical Engineer, from the Escuela Técnica Superior de Ingenieros Industriales of Valencia (Spain). In 1985 he got his PhD degree from the same institution. Since 2002, he has been a professor attached to the Department of Mechanical and Materials Engineering, where he teaches Theory of Machines and Mechanisms, Robotics and Mechanics. His research interests are currently focused on the design of parallel robots, identification of dynamic parameters and development of biomechanical models. He has been director / co-director of 7 doctoral theses and is the author of more than 80 papers published in JCR indexed journals.

Marina Vallés was born in Valencia, Spain in 1971. She received the B.S. degree in computer science in 1996, the M.S. degree in CAD/CAM/CIM in 1997 and the Ph.D. degree in automation and industrial computing in 2004 from Universitat Politècnica de València, Valencia, Spain. She is currently a Full Professor at the Systems Engineering and Automation Area of the Polytechnic University of Valencia. In the chapter of publications, 30 contributions between articles in journals and book chapters stand out and 84 Presentations in Congresses. Her research focuses on the implementation of controllers in real time and in limited resource systems.

Fernando J. Castillo was born in Almeria, Spain in 1976. He received the B.S. degree in Industrial Engineering in 2000, and the Ph.D. degree in Industrial Engineering (Mechatronics programme) in 2010 from Universidad de Castilla-La Mancha, Ciudad Real, Spain. He is currently Associate Professor at the Systems Engineering and Automation Area of the School of Industrial and Aerospace Engineering of Toledo. He is co-author of 36 papers in JCR journals and about 50 contributions to international congresses. His research is focused on robot and process control, parallel robots, cable-driven robots and legged robots.